A Non-Alkoxide Sol−Gel Method for the Preparation of Homogeneous Nanocrystalline Powders of $La_{0.85}Sr_{0.15}MnO_3$

Christopher N. Chervin,[†,‡] Brady J. Clapsaddle,[§] Hsiang Wei Chiu,[†] Alexander E. Gash,[§] Joe H. Satcher, Jr.,[§] and Susan M. Kauzlarich*[,†]

Department of Chemistry, University of California at Davis, One Shields Avenue, Davis, California 95616, and University Outreach and Chemistry and Materials Science Directorate, Lawrence Livermore National Laboratory, Livermore, California 94550

Received October 18, 2005. Revised Manuscript Received February 13, 2006

Homogeneous, nanocrystalline $La_{1-x}Sr_xMnO_3$ (LSM) powders, with $x \sim 0.15$, were synthesized with the epoxide addition sol−gel method. Through this simple technique, sol−gel materials were prepared from methanolic solutions of metal chlorides without the need for alkoxides, polymeric gel agents, or elaborate reaction schemes. The gels were dried in ambient conditions, resulting in mesoporous xerogels with networked nanostructures interconnecting particulate regions. Calcination of the dried gels resulted in the crystallization of single-phase LSM by 700 °C, after decomposition of intermediate hydroxide, chloride, and oxychloride compounds. SEM analysis indicated that the calcined powders were nanocrystalline and consisted of discrete particles, free of hard agglomeration. The average crystallite size and equivalent spherical diameter determined from XRD line broadening and BET analysis, respectively, were in good agreement with the SEM results (∼100 nm). The activation energies for the electronic conductivity from 1000 to 400 °C of sintered LSM xerogels were from 0.13 to 0.15 eV, in excellent agreement with previous reported results for LSM with $x \sim 0.15$.

Introduction

Doped lanthanum manganite ($LaMnO_3$), an intrinsic p-type conductor in the perovskite family, is a standard cathode of investigation for high-temperature solid-oxide fuel cells (SOFCs) and the most promising to date.[1−3] Electronic conductivity is enhanced by substitution of the La^{3+} site with divalent ions such as strontium or calcium.[4,5] Of the alkaline-earth dopants, strontium substitution is preferred for SOFC applications because the resultant perovskite forms stable compounds with high conductivity in the oxidizing atmosphere found at the cathode.[6] $La_{1-x}Sr_xMnO_3$ (LSM), where $x \sim 0.1-0.2$, provides maximum conductivity while maintaining mechanical and chemical stability with yttria-stabilized zirconia, the standard electrolyte used in SOFCs.[3,6−9]

Devices for these applications are often fabricated using particulate-based methods, such as screen-printing, slurry coating, spin coating, colloidal spray deposition, and tape-casting, followed by high-temperature sintering (on the order of 1000 °C).[10−13] The performance of the resultant cathode in SOFCs is dictated by the microstructure, which in turn is highly dependent on the morphology of the precursor oxide.[12,14] In the case of SOFC cathodes, fine-grained, homogeneous powder precursors have been identified as beneficial for optimizing electrode performance.[12] Furthermore, powders free of large (micrometer-sized) agglomerates are ideal for fabrication with particulate-based methods.[15,16] Nanoparticles, having larger surface energies than micrometer-sized particles, can potentially benefit ceramic processing by lowering sintering temperatures and creating higher surface area components with enhanced catalytic activity.[15,17−19] As a result, simple and effective routes for preparing agglomerate-free, homogeneous nanomaterials are desirable.

* To whom correspondence should be addressed.
† University of California at Davis.
‡ University Outreach, Lawrence Livermore National Laboratory.
§ Chemistry and Materials Science Directorate, Lawrence Livermore National Laboratory.

(1) Steele, B. C. H.; Heinzel, A. *Nature* **2001**, *414* (6861), 345−352.
(2) Singh, P.; Minh, N. Q. *Int. J. Appl. Ceram. Technol.* **2004**, *1* (1), 5−15.
(3) Minh, N. Q. *J. Am. Ceram. Soc.* **1993**, *76* (3), 563−588.
(4) Jonker, G. H. *Physica* **1954**, *20*, 1118−1122.
(5) Tanaka, J.; Takahashi, K.; Yukino, K.; Horiuchi, S. *Phys. Status Solidi A* **1983**, *80* (2), 621−630.
(6) Kuo, J. H.; Anderson, H. U.; Sparlin, D. M. *J. Solid State Chem.* **1990**, *87* (1), 55−63.
(7) Hammouche, A.; Siebert, E.; Hammou, A. *Mater. Res. Bull.* **1989**, *24* (3), 367−380.
(8) Yamamoto, O.; Takeda, Y.; Kanno, R.; Kojima, T. *SOFC-I, PV89-11*; Singhal, S. C., Ed.; The Electrochemical Society, Pennington, NJ, 1989; pp 242−253.
(9) Yokokawa, H.; Sakai, N.; Kawada, T.; Dokiya, M. *Solid State Ionics* **1990**, *40−41* (Pt. 1), 398−401.
(10) Pham, A.-Q.; Lee, T. H.; Glass, R. S. *SOFC-VI, PV99-19*; Singhal, S. C., Ed.; The Electrochemical Society, Pennington, NJ, 1999; pp 172−178.
(11) Endo, A.; Wada, S.; Wen, C. J.; Komiyama, H.; Yamada, K. *J. Electrochem. Soc.* **1998**, *145* (3), L35−L37.
(12) Sasaki, K.; Wurth, J. P.; Gschwend, R.; Godickemeier, M.; Gauckler, L. J. *J. Electrochem. Soc.* **1996**, *143* (2), 530−543.
(13) Murray, E. P.; Tsai, T.; Barnett, S. A. *Solid State Ionics* **1998**, *110* (3, 4), 235−243.
(14) Oestergaard, M. J. L.; Clausen, C.; Bagger, C.; Mogensen, M. *Electrochim. Acta* **1995**, *40* (12), 1971−1981.
(15) Mistler, R. E.; Twiname, E. R. *Tape casting: theory and practice;* Amercian Ceramic Society: Westerville, OH, 2000.
(16) Vanroosmalen, J. A. M.; Cordfunke, E. H. P.; Huijsmans, J. P. P. *Solid State Ionics* **1993**, *66* (3−4), 285−293.
(17) Tuller, H. L. *Solid State Ionics* **2000**, *131* (1, 2), 143−157.
(18) King, A. G. *Ceramic Technology and Processing;* William Andrew Publishing: New York, 2002.
(19) McColm, I. J. In *Ceramic Processing*; Terpstra, R. A., Pex, P. P. A. C., Vries, D., Eds.; Chapman and Hall: New York, 1995; pp 17−18.

10.1021/cm052301j CCC: $33.50
Published on Web 03/14/2006

LSM and related perovskites have been synthesized by numerous methods, including conventional solid-state synthesis, the Pechini method (polymeric precursors), coprecipitation, spray pyrolysis, and combustion synthesis.[16,20−23] Sol−gel methods, however, which are exceptional techniques for preparing homogeneous nanomaterials,[24] have not been extensively investigated. The lack of sol−gel methodology for the preparation of perovskite compounds is partly due to the difficulty in obtaining the necessary alkoxide precursors that are used in traditional sol−gel chemistry.[25] Often, the Pechini method and other polymeric precursor methods are referred to as sol−gel syntheses, but strictly speaking, these are inaccurate descriptions. Gel networks prepared with the Pechini route, for example, are created by polyesterification of citric acid (or other α-hydroxy carboxylic acids) and ethylene glycol (or other diols) and not distinctly created by inorganic oxolation and olation of the cation precursors (such as by hydrolysis and condensation).[25] Identifying nonalkoxide sol−gel methods, based on hydrolysis and condensation of cation precursors, could potentially expand the benefits of sol−gel chemistry to transition/rare-earth mixed metal oxide compounds. These benefits may include casting of ceramic devices, fabrication of monolithic components, and aerogel processing to produce mesoporous materials.[24−26]

Recently, Gash and co-workers have reported an alkoxide-free, sol−gel synthesis technique for preparing various transition, main group, and rare-earth metal oxides.[27−29] Through the use of an organic epoxide that acts as a proton scavenger, solutions of common hydrated metal salts undergo hydrolysis and condensation reactions to form metal oxide sol−gel materials.[29] The "epoxide addition method" eliminates the need for the often difficult preparation and handling of metal alkoxide precursors for nontraditional sol−gel metals and is complimentary to traditionally prepared sol−gel materials (i.e., SiO_2, TiO_2, Al_2O_3, etc.). Some examples of metal oxide gels prepared by the epoxide addition method include Ln_xO_y (Ln = all Ln^{3+}), Fe_2O_3, Cr_2O_3, Al_2O_3, Ga_2O_3, and ZrO_2, and the method has also proven useful in the synthesis of a variety of binary metal oxide systems, including yttria-stabilized zirconia.[28,30−33]

In the epoxide addition method the gel formation is facilitated by the proton-scavenging properties of the epoxide. The mechanism of proton scavenging is reported to occur in two steps: (1) reversible protonation of the epoxide ring by hydrolysis of the aquocation and (2) nucleophilic attack of the protonated epoxide ring by the counterion. The irreversible ring-opening reaction effectively removes a proton from solution, resulting in a homogeneous rise in the solution pH. The uniform rise in pH is accompanied by continued hydrolysis and condensation of the hydrolyzed cations to form gel networks.[29]

In this study, $La_{0.85}Sr_{0.15}MnO_3$ gels were prepared with an adaptation of the epoxide addition method using hydrated salts of La(III), Mn(II), and Sr(II) chlorides in methanol. We also investigate solutions of the individual cation salts and report difficulty in forming gels from pure Mn(II) or Sr(II) chloride. The difficulty in forming gels of divalent cations, which was previously reported by Gash et al.[34] and Long et al.,[35] is overcome in mixed metal systems containing the gel-forming La^{3+} species. This simple and effective way to prepare homogeneous LSM nanomaterials through a nonalkoxide sol−gel synthesis demonstrates the versatility of the epoxide addition method for the preparation of a variety of mixed metal oxide compounds.

Experimental Section

Synthesis. Sol−gel materials were prepared from metal chloride solutions by the epoxide addition method from $LaCl_3 \cdot 7H_2O$ (99.999%, Aldrich), $MnCl_2 \cdot 4H_2O$ (99.99%, Aldrich), $SrCl_2 \cdot 6H_2O$ (99%, Sigma-Aldrich), propylene oxide (99%, Aldrich), and methanol (HPLC grade, Mallinckrodt Chemicals). All chemicals were used as-received. Methanol was chosen as the solvent over commonly used water and ethanol because $SrCl_2 \cdot 6H_2O$ was not sufficiently soluble in ethanol at the desired concentration and in aqueous solutions $LaCl_3 \cdot 7H_2O$ was observed to form precipitates with epoxide addition.

Gels were prepared by dissolving the appropriate amounts of metal chlorides in methanol at room temperature followed by stirring for 1 h. Subsequently, propylene oxide was added rapidly and the solutions were stirred vigorously until gelation or precipitation occurred. Four metal chloride systems were investigated: La^{3+}, Mn^{2+}, Sr^{2+}, and $La^{3+}/Sr^{2+}/Mn^{2+} = 0.85/0.15/1$ (mol/mol/mol). The four systems will be referred to as La, Mn, Sr, and LSM gels, respectively. In a typical synthesis of an LSM gel, $LaCl_3 \cdot 7H_2O$ (11.3640 g, 0.0306 mol), $MnCl_2 \cdot 4H_2O$ (7.1247 g, 0.0360 mol), and $SrCl_2 \cdot 6H_2O$ (1.4397 g, 0.0054 mol) were dissolved in methanol (43.26 g, 1.350 mol) such that the total cation concentration, $[M^{x+}]$, was 1.3 m/L. Following complete dissolution of the salts, propylene oxide (PO; 37.65 g, 0.6482 mol) was added such that the molar ratio of PO to metals (R_{epox}) was 9 and the container was immediately capped. The resultant solution was stirred until gelation occurred. The gel points for the reactions were qualitatively determined as the point at which the sols no longer flowed under the influence of gravity when the reaction containers were tilted. *Caution: some gas evolution is observed following epoxide addition and the cap should be opened occasionally during the first minute*

(20) Gaudon, M.; Laberty-Robert, C.; Ansart, F.; Stevens, P.; Rousset, A. *Solid State Sci.* **2002**, *4* (1), 125−133.
(21) Hammouche, A.; Siebert, E.; Hammou, A. *Mater. Res. Bull.* **1989**, *24* (3), 367−380.
(22) Song, K. S.; Cui, H. X.; Kim, S. D.; Kang, S. K. *Catal. Today* **1999**, *47* (1−4), 155−160.
(23) Aruna, S. T.; Muthuraman, M.; Patil, K. C. *J. Mater. Chem.* **1997**, *7* (12), 2499−2503.
(24) Brinker, C. J.; Scherer, G. W. *Sol−Gel Science;* Academic Press: Boston, 1990.
(25) Livage, J.; Henry, M.; Sanchez, C. *Prog. Solid State Chem.* **1988**, *18* (4), 259−341.
(26) Hench, L. L.; West, J. K. *Chem. Rev.* **1990**, *90* (1), 33−72.
(27) Gash, A. E.; Satcher, J. H., Jr.; Simpson, R. L. *Chem. Mater.* **2003**, *15* (17), 3268−3275.
(28) Gash, A. E.; Tillotson, T. M.; Satcher, J. H., Jr.; Hrubesh, L. W.; Simpson, R. L. *J. Non-Cryst. Solids* **2001**, *285* (1−3), 22−28.
(29) Gash, A. E.; Tillotson, T. M.; Satcher, J. H., Jr.; Poco, J. F.; Hrubesh, L. W.; Simpson, R. L. *Chem. Mater.* **2001**, *13* (3), 999−1007.
(30) Chervin, C. N.; Clapsaddle, B. J.; Chiu, H. W.; Gash, A. E.; Satcher, J. H.; Kauzlarich, S. M. *Chem. Mater.* **2005**, *17* (13), 3345−3351.
(31) Clapsaddle, B. J.; Gash, A. E.; Satcher, J. H.; Simpson, R. L. *J. Non-Cryst. Solids* **2003**, *331* (1−3), 190−201.
(32) Clapsaddle, B. J.; Sprehn, D. W.; Gash, A. E.; Satcher, J. H.; Simpson, R. L. *J. Non-Cryst. Solids* **2004**, *350*, 173−181.
(33) Clapsaddle, B. J.; Sprehn, D. W.; Gash, A. E.; Satcher, J. H.; Simpson, R. L. *Abstr. Pap. Am. Chem. Soc.* **2005**, *229*, U1094−U1095.
(34) Gash, A. E.; Satcher, J. H.; Simpson, R. L. *J. Non-Cryst. Solids* **2004**, *350*, 145−151.
(35) Long, J. W.; Logan, M. S.; Carpenter, E. E.; Rolison, D. R. *J. Non-Cryst. Solids* **2004**, *350*, 182−188.

to prevent pressure buildup in the container and potential splashing of the reaction solvent.

Following gelation, the gels were aged for 24 h under ambient conditions in closed containers. The aged gels were then washed with ethanol for 3 days, with fresh ethanol exchanged daily. Xerogels were prepared by drying wet gels in air at room temperature for 24 h followed by additional drying at 65 °C in air for 24 h. LSM xerogels were ground to a fine powder in a mortar and pestle and then calcined in air at various temperatures to examine the crystalline products, resulting morphology, and elemental composition. The dwell times at the desired temperature were 1 h and the heating and cooling ramps were 2 and 4 °C/min, respectively.

Physical Characterization. Powder X-ray diffraction patterns of as-prepared La, Mn, and LSM xerogels and calcined LSM were measured using a Scintag PAD V diffractometer operating at 40 A and 45 keV with Cu Kα radiation ($\lambda = 1.54056$ Å). The patterns were collected with a 0.02 step and 5 s dwell time at each step. The cell parameters and average crystallite size of an LSM xerogel calcined at 700 °C was determined from Rietveld refinement using GSAS refinement software. The XRD pattern for the refined sample was collected with a 0.02 step and 10 s dwell times at each step.

Thermal analysis of LSM xerogels were performed by simultaneous differential scanning calorimetry (DSC) and thermogravimetric analysis (TGA) using a Netzsch 449 Thermal Analyzer in the temperature range of 25 to 1000 °C under flowing air or oxygen with a 10 °C/min ramp. Fourier transform infrared spectroscopy (FT-IR) of the evolved gas produced during the thermal analysis was measured by directing the gas flow from the thermal analyzer to a Bruker Equinox 55 TGA-IR spectrometer equipped with a solid-state detector. Data were acquired with 16 scans in the range 4000−400 cm^{-1} with a 4 cm^{-1} resolution and 1 s scans. A 64 scan background of the atmosphere gas was run prior to heating the sample and subtracted from the resulting spectrum.

Surface area, pore volume, and pore size analyses were performed using an ASAP 2000 surface area analyzer (Micromeritics Instrument Corp.). Prior to analysis, samples of approximately 0.1−0.2 g were heated to 200 °C under vacuum (10^{-5} Torr) for at least 24 h to remove adsorbed species. Nitrogen adsorption data were taken at five relative pressures from 0.05 to 0.20 at 77 K, and the surface area was calculated using BET (Brunauer−Emmett−Teller) theory. Average pore size and pore volumes were calculated using the BJH (Barrett−Joyner−Halenda) method from the desorption branch of the isotherm.

Xerogel morphologies were examined with scanning electron microscopy (SEM) and bright field transmission electron microscopy (TEM). TEM images were collected for as-prepared La, Mn, and LSM xerogels and SEM images were collected for calcined LSM xerogels. SEM measurements were made using a Philips 30XL FEG SEM operated at 5 keV. SEM samples were prepared by applying drops of methanol suspensions of the respective powders on to aluminum SEM stubs heated to ∼120 °C, followed by drying at 120 °C overnight. TEM analysis was performed using a Philips CM-12 TEM, operating at 100 keV. TEM samples were prepared by dipping holey carbon-coated 400-mesh grids into methanol colloids of the respective powders, followed by drying at 120 °C overnight.

Elemental analysis of LSM xerogels as-prepared and after calcination at 800 and 1000 °C were determined by inductively coupled plasma−atomic emission spectroscopy (ICP-AES) by Galbraith Laboratories of Knoxville, TN.

Measurement of Electronic Conductivity of LSM. The electronic conductivity as a function of temperature for xerogel-derived LSM powder was measured using the four-probe technique of van der Pauw.[36] Pellets were prepared from an LSM xerogel powder synthesized with $[M^{x+}] = 1.3$ m/L and $R_{epox} = 9$. Prior to pressing pellets the powder was calcined at 1000 °C for 1 h followed by ball-milling in ethanol overnight with 8 wt % poly(vinyl butyral-*co*-vinyl alcohol-*co*-vinyl) acetate (PVB; Aldrich Chemicals) binder using yttria-stabilized zirconia mill media (Inframat Advanced Ceramics) in a polyethylene bottle. The milled powder was dried at 90 °C for ∼12 h and lightly ground in a mortar and pestle. The powder was then isostatically pressed into rectangular-shaped pellets at 920 bar and sintered in air at 1400 °C for 3 h. Additionally, one pellet was prepared from calcined LSM xerogel powder without PVB binder and sintered at 1400 °C for 3 h to examine the effect of the binder on the pellet density.

Platinum voltage and current electrodes were applied to the sintered pellets as a paste (Heraeus, CL11-5349) and fired at 900 °C for 30 min. The sintered pellets were approximately 1.75 cm long and 0.1 cm^2 in cross section, and the voltage electrode separation was 0.9 cm. Platinum wires were attached to the electrodes with Pt paste followed by an additional sintering at 1000 °C for 30 min. The electrochemical leads were connected to the platinum wires and the pellets were placed in quartz tubes.

Conductivity measurements were made in a tube furnace under flowing air (0.5 L/min) from 1000 to 300 °C at 50 °C intervals. For each temperature, an ac current of 1 mA at 400 Hz and an amplitude of 20 mA was applied with a Solartron SI 1260 impedance/gain phase analyzer and Solartron SI 1287 electrochemical interface. The resulting ac impedances were collected for 5 min at each temperature and the average sample resistances were determined. For comparison, steady-state dc voltage−current data were also collected at selected temperatures and agreed with the ac impedance results.

Results and Discussion

Sol−Gel Chemistry of La^{3+}, Mn^{2+}, Sr^{2+}, and LSM Solutions. The sol−gel synthesis of LSM and the individual La, Mn, and Sr systems were investigated. The results for the individual cations varied, reflecting the different reactivity of each species. The divalent cations formed precipitates; however, the rate of precipitation varied dramatically. Precipitation was rapid in Sr(II) chloride solutions, occurring in <2 min, whereas with Mn(II) chloride a sol formed that persisted for at least 40 min before slowly precipitating. Conversely, monolithic gels readily formed for both pure La(III) chloride and the LSM system. The sol−gel synthesis of the individual La^{3+}, Mn^{2+}, and Sr^{2+} cations will be discussed briefly prior to discussion of LSM.

PO addition to a methanolic solution of $LaCl_3 \cdot 7H_2O$ ($[La^{3+}] = 1.3$ m/L, $R_{epox} = 9$) resulted in the formation of a white, monolithic gel in approximately 6 min. The La gelation point was preceded by a notable increase in the solution viscosity and the formation of a cloudy, white sol. After aging and washing in ethanol, the gel was dried, resulting in white materials that were soft and easily ground to fine powders in a mortar and pestle. The ability to form La gels in methanol was anticipated based on previous success with lanthanide chlorides in ethanol solvent.[33]

The addition of PO to a methanolic solution of $MnCl_2 \cdot 4H_2O$ ($[Mn^{2+}] = 1.3$ m/L, $R_{epox} = 9$) resulted in the formation of a tan sol in approximately 2 min, which slowly became

(36) Van der Pauw, L. J. *Philips Res. Rep.* **1958**, *13*, 1−9.

viscous and took on a gel-like appearance. After ~40 min the gel slowly separated from the solvent. The product appeared to have characteristics of both a gel and a precipitate; however, based on TEM results that will be presented later, it will be called a precipitate. While the tan precipitate was aged overnight in the closed container, the solvent layer adsorbed into the precipitate forming a wet, caked material. Following aging/washing in ethanol for several days, the precipitate turned dark brown and appeared to be homogeneous. The brown color is attributed to oxidation of some Mn^{2+} to Mn^{3+} in the presence of air.[37] The air-dried materials were easily ground into fine brown powders with a mortar and pestle.

The addition of PO to a methanolic solution of $SrCl_2 \cdot 6H_2O$ ($[Sr^{2+}] = 1.3$ m/L, $R_{epox} = 9$) resulted in the formation of a white precipitate within 1.5 min. The precipitate was distinctly different from the precipitate of the Mn system, in that it rapidly settled out of solution without observable formation of a sol. The product was not characterized further.

LSM gels with a La/Sr/Mn molar ratio of 0.85/0.15/1 were prepared in methanol ($[La^{3+}] + [Mn^{2+}] + [Sr^{2+}] = 1.3$ m/L, $R_{epox} = 9$). The reaction resulted in the formation of a viscous white sol in 6 min, which solidified to a monolithic white gel by 8.5 min. During the washing step (several days), the monolith underwent a gradual color change to dark brown, similar to that of the Mn precipitate. The texture, however, was similar to the pure La gel, but appeared slightly grainy. The emergence of the dark brown color in the LSM gel, distinctly different from the white La gels, indicates that Mn^{x+} is present, whereas the formation of a gel is indicative of the La component. The presence of Sr^{2+} is not observable from the gel color (Sr compounds tend to be white) or texture, and therefore, identification of Sr^{2+} in the gel requires elemental analysis, which will be presented later. Drying the LSM gel resulted in a partially monolithic xerogel that was easily broken into fine pieces. Further grinding in a mortar and pestle produced ultrafine powder.

Previously, Gash and co-workers reported difficulty in preparing sol−gel materials with nitrate salts of M^{2+} ions of the late 3d transition metals ($M = Ni^{2+}$, Co^{2+}, Zn^{2+}, and Cu^{2+}) and more recently success with Ni(II) chloride.[28,34] Therefore, it was not surprising to observe precipitates in the Sr^{2+} and Mn^{2+} systems compared with the distinct gels formed with La^{3+}. Protonation of the epoxide ring requires the aquocation to act as an acid and in general the acidity of aquocations depends on charge with 4+ cations typically more acidic than 3+ cations and 2+ cations being weakly acidic.[38] The inability to form gels with divalent cations is possibly related to their lower acidity compared with trivalent and tetravalent cations; however, the counterion also appears to play a role.[34] In general, chloride salts are more effective precursors for the epoxide addition method than nitrate salts because of the greater nucleophilic nature of chloride. Long et al. reported the inability to gel Mn(II) chloride in ethanol using the epoxide, epichlorohydrin, but succeeded in preparing Fe−Mn gels with a 1:2 Mn:Fe composition using similar reagents.[35] In that case, the Mn was believed to incorporate into the Fe gel structure, despite the inability to form "neat" MnO gels.

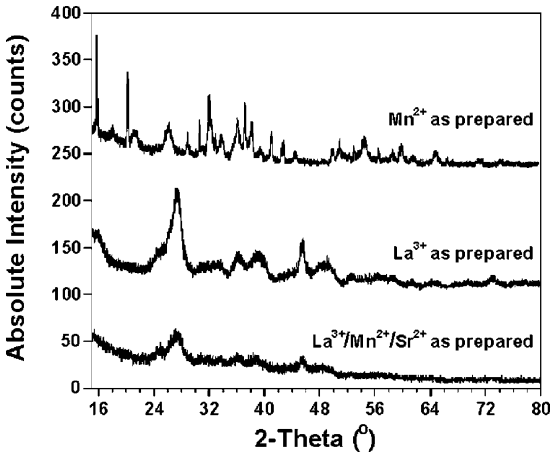

Figure 1. Powder XRD patterns of as-prepared xerogels. From top to bottom: Mn^{2+}, La^{3+}, and $La^{3+}/Sr^{2+}/Mn^{2+} = 0.85/0.15/1$ (mol/mol/mol). Samples were prepared with total $[M^{x+}] = 1.3$ m/L and $R_{epox} = 9$. Absolute intensities are shown and the individual patterns are offset on the graph for clarity.

The objective of this work, supported by the results of Long et al., was to prepare a multicomponent oxide gel in which divalent cations are incorporated into the gel network of a gel-forming rare-earth metal. We are interested in LSM for fuel cell applications, but recognize that this sol−gel method can be general for preparing a variety of perovskites and other technologically significant materials. XRD and microscopy results of the La, Mn, and LSM gels will be presented; however, only the LSM system will be characterized extensively.

Powder X-ray Diffraction. Figure 1 shows powder XRD patterns for as-prepared xerogels of the La, Mn, and LSM systems. The three diffraction profiles were measured with identical scan times and are offset on the graph for clarity. The La xerogel was crystalline with broad peaks in the diffraction pattern. The low intensity and poorly defined peaks indicate the phases are nanocrystalline and significant amorphous material is likely present. These peaks were indexed as a mixture of $La(OH)_3$, $LaCl_3(H_2O)_3$, and $La(OH)_2Cl$ (PDF #'s 06-0585, 82-1200, and 70-2139, respectively). The formation of hydroxides, chlorides, and hydroxychlorides is reasonable considering the aqueous chemistry for trivalent cations in which hydrolysis products are often hydroxo and aquo-hydroxo complexes.[25] In this case, the solvent is not aqueous but the precursor salts are hydrated and water is likely present as inner coordination sphere ligands because it is a better nucleophile toward La^{3+} than is chloride or methanol.[39] Chloride is observed in the condensation products and this may vary with reaction concentration. A more detailed study of the La system may reveal variation in chloride products as a function of solvent and inorganic salt concentration.

(37) Cotton, F. A.; Wilkinson, G. In *Advanced Inorganic Chemistry*; John Wiley and Sons: New York, 1988; p 758.
(38) Burgess, J. In *Metal Ions in Solution*; Ellis Horwood Limited: Chichester, 1978; p 259.
(39) Smith, L. S., Jr.; McCain, D. C.; Wertz, D. L. *J. Am. Chem. Soc.* **1976**, *98* (17), 5125−5128.

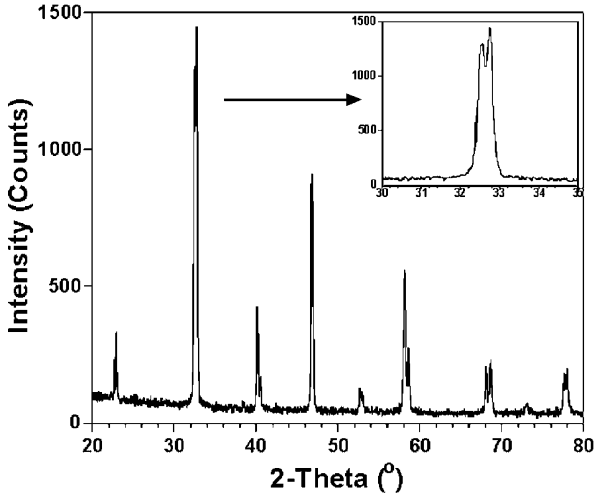

Figure 2. Powder XRD patterns for an LSM xerogel calcined at 700 °C for 1 h. The hexagonal structure for LSM (space group $R\bar{3}cH$) is observed. The inset shows the splitting of the (110) and (104) reflections.

The powder XRD of the Mn gel precipitate, shown in Figure 1, indicates that a multiple phase crystalline product resulted from epoxide addition to the Mn(II) chloride solution. Broad, poorly defined peaks corresponding to Mn_3O_4, MnO(OH), and MnO (PDF #'s 24-0734, 41-1379, and 04-0326, respectively) and sharp peaks from hydrated $MnCl_2$ (PDF # 60-5458) are observed. The precursor Mn^{2+} was partially oxidized to Mn^{3+}, as indicated by the presence of Mn_3O_4 and MnO(OH) in the product. The brown color of the gel precipitate is also consistent with oxidation of Mn(II) hydroxide in air to form brown products.[37]

The as-prepared LSM xerogel displayed a diffraction pattern similar to that of the pure La gel but with lower peak intensities. The presence of Mn in the xerogel, indicated by the brown color, did not change the observed phases; however, the reduced intensities of the observed peaks indicate a more amorphous nature of the LSM xerogel compared with that of the pure La xerogel. The absence of additional peaks in the LSM sample suggests that either the Mn and Sr mix with La in the gel structure or they form separate amorphous phases undetectable with powder XRD. The presence of Mn and Sr, confirmed by both the formation of crystalline LSM upon calcination and bulk elemental analysis, will be discussed.

Calcination of the brown LSM xerogel to 700 °C resulted in decomposition of the mixed phase hydroxides and chlorides (as-prepared xerogel) to produce a crystalline, black powder. The diffraction pattern, shown in Figure 2, demonstrates that the xerogel crystallized into a single-phase perovskite with reflections corresponding to the rhombohedral (hexagonal) structure for LSM (PDF# 62-6052), space group $R\bar{3}cH$. This structure is consistent with $La_{1-x}Sr_xMnO_3$ for $0.1 \leq x \leq 0.4$, suggesting that Sr^{2+} is present in the xerogel.[40] Below $x = 0.1$ the structure is reported to be orthorhombic.

The powder pattern was refined with the Rietveld method using the GSAS refinement software.[41] The cell parameters

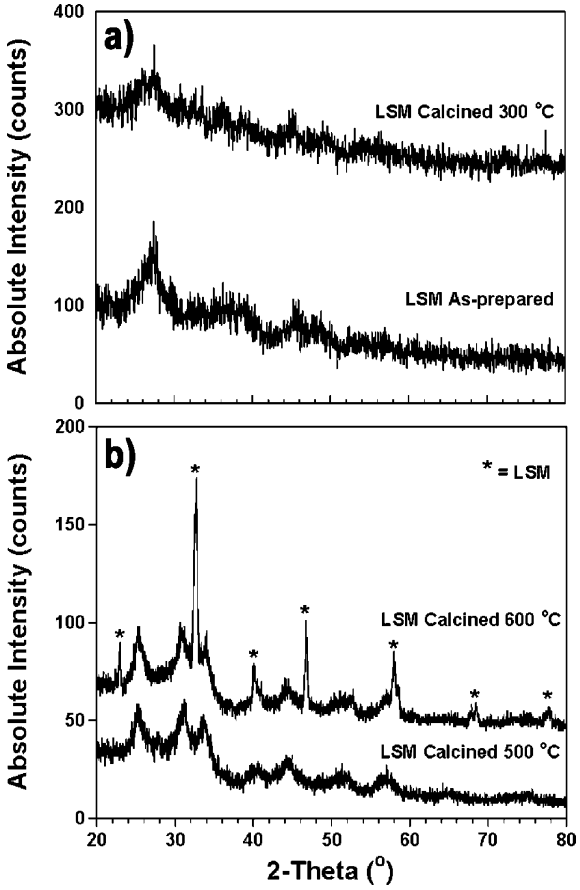

Figure 3. Powder XRD patterns for an LSM xerogel (a) as-prepared (bottom) and calcined at 300 °C for 1 h (top) and (b) calcined for 1 h at 500 °C (bottom) and 600 °C (top). LaOCl is observed above 500 °C and the major peaks associated with the hexagonal LSM structure are evident at 600 °C.

were determined to be $a = b = 5.5087(8)$ and $c = 13.352(8)$. The calculated average crystallite size was 94 nm, determined from Gaussian peak broadening using

$$P = \frac{18000K\lambda}{\pi\sqrt{Lp(8 \ln 2)}} \quad (1)$$

where P is the crystallite size in Å, K is the Scherrer constant (taking to be 1), λ is the X-ray wavelength (1.54056 Å), and Lp is the refined Gaussian profile term.[41]

The crystallization of LSM from the as-prepared xerogel was preceded by decomposition of the hydroxide and chloride compounds and the formation of an intermediate lanthanum oxychloride phase. The phase changes were observed with XRD of the xerogel calcined at 300, 500, and 600 °C. The powder was also observed to go through a color change from brown to dark brown at 600 °C, and finally, black at 700 °C. The black powder at 700 °C is the expected color for $La_{0.85}Sr_{0.15}MnO_3$ and the darkening of the powder at 600 °C occurs because the LSM phase has begun to crystallize, as confirmed by XRD shown in Figure 3.

Figure 3a shows XRD patterns of an LSM xerogel before and after calcination at 300 °C for 1 h. The diffraction pattern of the brown as-prepared LSM xerogel was similar to that of the La xerogel and had peaks associated with lanthanum hydroxides, chlorides, and hydroxy-chlorides. After calcination at 300 °C, the diffraction peaks are still discernible;

(40) Bindu, R. *Eur. Phys. J. B* **2004**, *37* (3), 321−327.
(41) Larson, A. C.; Von Dreele, R. B. *Los Alamos National Laboratory Report LAUR* **2000**, 86-748.

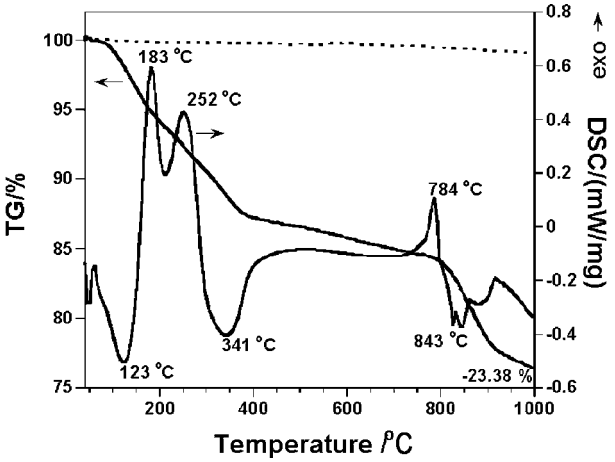

Figure 4. TGA/DSC scan for an as-prepared LSM xerogel (solid lines) heated in oxygen at 10 °C/min. Additionally, the TGA scan for the LSM xerogel precalcined at 700 °C for 1 h is shown (dashed line). The major weight loss observed above 800 °C for the as-prepared xerogel is not observed in the precalcined sample.

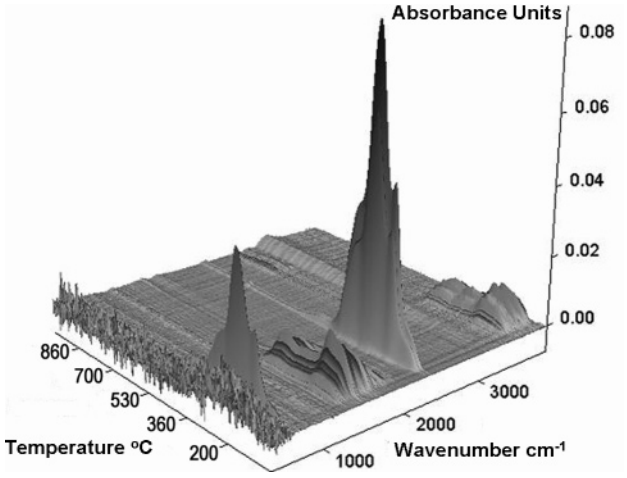

Figure 5. Evolved gas FT-IR run simultaneously with the TGA/DSC scans of the as-prepared xerogel in Figure 4. The major bands occurring below 400 °C are associated with water and CO_2.

however, they have decreased in intensity, indicating that the compounds are decomposing with heating. The decomposition of the LSM xerogels likely occurs by condensation of chemisorbed hydroxyl groups, leading to increased M−O−M bond formation.[26]

Figure 3b shows XRD patterns for the LSM xerogel after calcination at 500 and 600 °C for 1 h. Following heating to 500 °C, the hydroxide and chloride compounds have completely decomposed and new peaks indexed as LaOCl (PDF # 64-7261) are observable in the diffraction profile. The LaOCl peaks are present after heating to 600 °C and, additionally, intense peaks associated with the hexagonal perovskite structure (LSM) emerge. By 700 °C, the LaOCl has decomposed and the single-phase perovskite is formed (Figure 2). Note though the measurement conditions were identical, the peak intensities were significantly greater for the perovskite structure at 700 °C (Figure 2) compared with those of the precursor phases (Figures 3a and 3b). The phases present prior to 700 °C are poorly crystalline and likely mixed with significant amounts of amorphous materials.

Thermal Analysis. Figure 4 shows a typical TGA/DSC scan for an LSM xerogel heated to 1000 °C in oxygen. The DSC scan has several exothermic and endothermic peaks that are associated with weight loss in the TGA scan. The first event is endothermic with a peak maximum at 123 °C, followed by a broad exotherm with two peaks at 180 and 250 °C. A second endotherm is observed with a maximum at 341 °C. These four peaks correspond to a steady weight loss of 13% by 400 °C. The DSC scan is featureless from 400 to 770 °C but TGA revealed an additional 4% weight loss occurring gradually from 400 to 800 °C. A sharp exothermic feature at 784 °C and a subsequent broad endothermic feature from 796 to 915 °C are observed. The high-temperature endotherm corresponds to a weight loss in the sample of 6%. The total weight loss in the LSM xerogel calcined to 1000 °C was 23%.

Also shown in Figure 4 is a TGA scan for the LSM xerogel precalcined to 700 °C for 1 h prior to thermal analysis (dashed line). The weight loss over the entire temperature range is <1%, indicating that the observed 6% weight loss from 800 to 1000 °C for the as-prepared xerogel (solid line) is related to the fast heating rate (10 °C /min) and absence of a high-temperature dwell period. These results correspond with the XRD data, which shows decomposition of hydroxide and chloride compounds below 700 °C prior to crystallization of the single-phase hexagonal structure. Additionally, based on XRD analysis, the hexagonal phase present at 700 °C did not change when the sample was calcined to 1000 °C, supporting the contention that the weight loss occurred below 700 °C.

Evolved gas FT-IR run simultaneously with the TGA/DSC scans of the as-prepared xerogel is shown in Figure 5. The resultant absorbance plot shows peaks associated with water and CO_2. The asymmetrical stretching and bending modes for CO_2 are seen as a relatively sharp band at 2352 and 662 cm^{-1} throughout the temperature range 50−390 °C. A broad band associated with symmetrical and asymmetrical OH stretching in water occurs from 3550 to 3964 cm^{-1} in the same temperature range as the CO_2 bands. The water and CO_2 peaks occur simultaneously, corresponding with the weight loss up to 400 °C. The broad endotherm below 200 °C is attributed to desorption of tightly bound water or organic compounds and the exotherm between 180 and 250 °C to both pyrolysis of organic compounds and condensation of hydroxyl groups on the gel. The pyrolysis is evident by the CO_2 observed in the FT-IR data, whereas condensation is supported by the observed elimination of hydroxyl compounds in XRD patterns of xerogels heated to 500 °C (Figures 3a and 3b).

The 6% weight loss that occurred above 800 °C did not provide a gaseous species that could be detected by FT-IR. The reason for this is not known; however, the evolved gas may not correspond to IR active species or they may have condensed in the outgas tubing, which is maintained at ∼100 °C, before reaching the IR detector. Considering the presence and subsequent decomposition of La oxychloride above 500 °C, it is likely the 6% weight loss is from chloride-containing compounds. This is supported by elemental analysis, which demonstrates a dramatic decrease in chloride in the calcined product compared with that of the as-prepared xerogel.

Table 1. ICP-AES Results for LSM Xerogels

sample	La/Sr	(La + Sr)/Mn	Cl (wt %)	C (wt %)	x in $La_{1-x}Sr_xMnO_3$
LSM-U (800 °C)	6.18	1.02	2.73	<0.5	0.14
LSM-W (800 °C)	7.03	1.00	1.23	<0.5	0.12
LSM-W (1000 °C)	6.73	0.99	<20 ppm	<0.5	0.13
LSM-W (as-prepared)	6.50	0.99	10.80	2.06	0.13
expected	5.67	1.00			0.15

Elemental Analysis. The elemental compositions of as-prepared and calcined LSM xerogels were determined by ICP-AES. Additionally, the effect of the washing step on composition and chloride content was investigated. Two separate gels were prepared from the same precursor solution ($[La^{3+} + Mn^{2+} + Sr^{2+}] = 1.3$ m/L and $R_{epox} = 9$). After the chloride salts were dissolved in methanol, the solution was divided into equal portions and each portion was gelled with identical amounts of PO under similar ambient conditions. After gelation, one sample was washed with ethanol for several days before drying, whereas the other sample was immediately dried. The two samples will be referred to as LSM-W and LSM-U for the washed and unwashed samples. Each powder was calcined at 800 °C for 1 h before determining the elemental compositions. LSM-W was also analyzed after calcination at 1000 °C for 1 h.

Elemental analysis results for calcined LSM-W and LSM-U and an as-prepared LSM xerogel are presented in Table 1. The elemental compositions are listed as molar ratios for metals and weight percents for chloride and carbon. All of the samples showed significant amounts of Sr and Mn present, indicating the elements were incorporated into the gels and were not significantly removed during washing. However, the ratio of La/Sr was slightly higher for LSM-W than for LSM-U, suggesting that the washing process did remove some Sr^{2+}. Both samples had (La + Sr)/Mn ratios of ~1.0 and the chloride content for LSM-W and LSM-U were 1.23 and 2.73%, respectively. Therefore, washing the wet gel appears to be beneficial for lowering chloride byproducts from the calcined sample. Further calcination of LSM-W to 1000 °C did not alter the elemental composition of La, Sr, and Mn; however, the chloride content decreased to <20 ppm. The three calcined samples had carbon contents below the detection limit of the analysis.

The as-prepared LSM xerogel included in Table 1 was prepared and washed under reaction conditions similar to those for LSM-W. The results show that the La, Sr, and Mn compositions are similar between the samples, demonstrating that the synthetic method is reproducible and that the metals present in the as-prepared gel were retained during calcination to 1000 °C. The chloride and carbon content, however, were significantly higher in the as-prepared xerogel, 10.80 and 2.06 wt %, respectively. The significant reduction of chloride with calcination to 800 °C is consistent with the XRD (Figure 3) and TGA/DSC (Figure 4), which show decomposition of precursor chlorides and significant weight loss occurring in the xerogel up to 700 °C. Furthermore, calcination to 1000 °C reduces the chloride content to ppm. In general, applications involving LSM require sintering steps of greater than 1000 °C and, therefore, the chloride will be greatly removed in these devices.

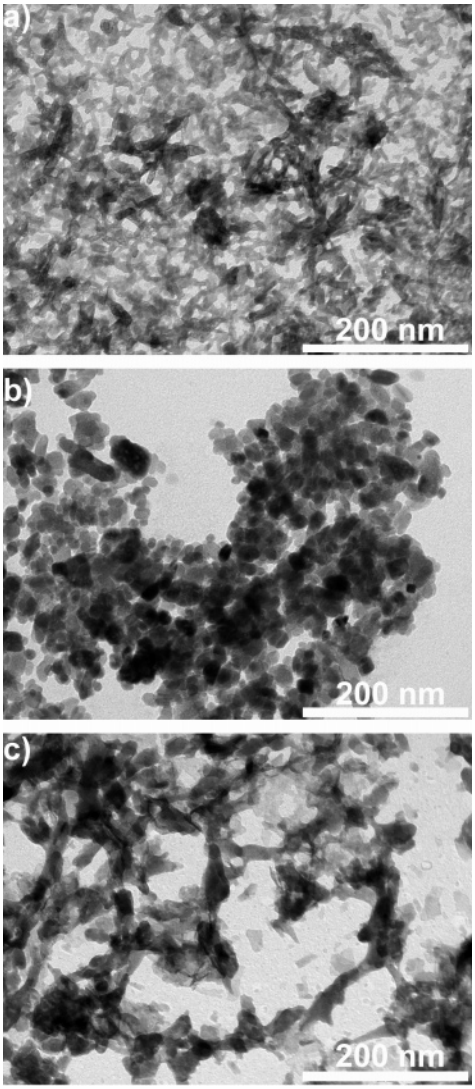

Figure 6. Bright field TEM micrographs of as-prepared xerogels: (a) La, (b) Mn, and (c) LSM. The gels were prepared with total $[M^{x+}] = 1.3$ m/L and $R_{epox} = 9$.

The Sr^{2+} substitution was determined for the xerogels in Table 1, assuming that La + Sr = 1 on the A-site of the $(La_{1-x}Sr_x)MnO_3$ structure.[42] LSM-U and LSM-W calcined to 800 °C had $x = 0.14$ and 0.12, respectively, compared with the expected value $x = 0.15$. LSM-W calcined to 1000 °C had $x = 0.13$ and the as-prepared xerogel, though not a perovskite until after calcination, had a metal composition corresponding to $x = 0.13$. These results indicate that the Sr and Mn incorporate into the gel structure and remain throughout calcination. The observed Sr deficiency can be minimized by avoiding or reducing the washing step.

Electron Microscopy of As-Prepared Gels. The morphologies of as-prepared La, Mn, and LSM xerogel powders were examined with TEM. The La xerogel, shown in Figure 6a, displayed a mesoporous, networked structure formed by hydrolysis and condensation of the precursor cations.[26] The networks are relatively short and interconnect particulate regions in the xerogel. The material appears homogeneous and it is difficult to discern the different phases that were observed in XRD.

(42) Kertesz, M.; Riess, I.; Tannhauser, D. S.; Langpape, R.; Rohr, F. J. *J. Solid State Chem.* **1982**, *42* (2), 125−129.

The Mn precipitate is shown in Figure 6b. Discrete nanoparticles with inhomogeneous size and shape are observed. In this case, the inhomogeneity may be a direct observation of the multiple phases that are seen in the XRD pattern. The particles are relatively large compared with the La xerogel and lack networked structures. Following epoxide addition, the viscosity of the Mn(II) chloride solution slowly increased, giving it a gel-like appearance. The TEM results suggest that the increased viscosity was not related to the formation of a gel network, but more likely due to the increase in colloid size and concentration. Eventually, the colloids became too large or too concentrated to remain stable and slowly precipitated.

The LSM xerogel, shown in Figure 6c, has a morphology intermediate between the networked structure of the La gel and the discrete particles formed with the Mn precipitate. The networks have larger widths than those observed in the La xerogel and interconnect inhomogeneous particulate regions. It is not possible, from the TEM results, to determine if the cations mix on an atomic scale or form segregated phases connected by the network. Considering the different reaction rates of the individual cations, however, the La network may form initially, providing a scaffold that incorporates the divalent cation colloids on a nanoscale. Furthermore, the XRD pattern for the xerogel does not show phases associated with the divalent cations, which would provide direct evidence of phase segregation. The relatively low crystallization temperature of LSM from the xerogel (700 °C), which is common for wet chemical methods that mix elements on the atomic scale, suggests that the materials are intimately mixed.[43]

Electron Microscopy of Calcined LSM Xerogels. Calcination removes the inhomogeneous, networked morphology of the LSM xerogel. The decomposition observed in XRD and TGA/DSC is accompanied by the formation of nanoparticulate, crystalline LSM. SEM micrographs of the LSM xerogel calcined to 700 °C are shown in Figure 7. The low-magnification micrograph, shown in Figure 7a, demonstrates the homogeneous size distribution and agglomerate-free nature of the calcined material. The absence of hard agglomerates, which are formed by particle−particle sintering, may be related to the porous nature of the as-prepared xerogel precursor. The interparticle contact is minimized by the open structure, thereby preventing the formation of large, partially sintered agglomerates. The significant decomposition and weight loss that is coincident with calcination may also help in preventing the growth of agglomerates. This sol−gel method for preparing LSM was highly reproducible, and in all cases, similar morphologies were obtained.

The high-magnification micrograph in Figure 7b highlights the particulate morphology of the crystallized LSM. The nanoparticles are primarily spherical; however, some elongated morphologies are present, suggesting that interparticle growth occurred during calcination. The particle diameters are approximately 100 nm. Calcination to 1000 °C resulted in increased particle growth without observed change in morphology, as shown in an SEM micrograph in Figure 7c. The particle sizes after calcination at 1000 °C were approximately 200 nm. Furthermore, as with the lower calcination temperature, hard agglomerates were not observed.

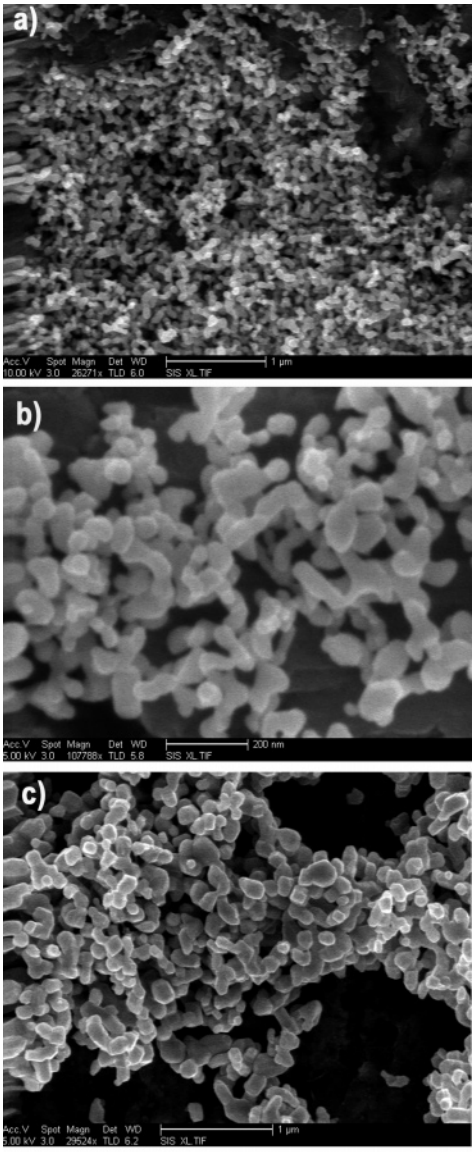

Figure 7. SEM micrographs of a calcined LSM xerogel: (a) 700 °C for 1 h at low magnification, (b) 700 °C for 1 h at high magnifications, and (c) 1000 °C for 1 h.

BET/BJH Surface Area Analysis. The surface area, average pore size, and pore volume were determined for an LSM xerogel. The BET surface area for the as-prepared xerogel powder was 216 m^2/g and the average pore size and pore volume were 15 nm and 1.01 mL/g. Therefore, xerogel processing of the resulting gels produced a high surface area material with a mesoporous structure (pore diameters = 2−50 nm), consistent with the TEM results.[44] The adsorption−desorption isotherms for the xerogel were Type IV with desorption branch hysteresis, typical of mesoporous materials.[44]

The BET surface area for the xerogel calcined at 700 °C for 1 h was 9.0 m^2/g. Using the surface area and assuming

(43) Tai, L. W.; Lessing, P. A. *Powder Metall. Int.* **1991**, *23* (5), 301−304.

(44) Sing, K. S. W.; Everett, D. H.; Haul, R. A. W.; Moscou, L.; Pierotti, R. A.; Rouquerol, J.; Siemieniewska, T. *Pure Appl. Chem.* **1985**, *57* (4), 603−619.

all particles are spherical, the average particle size (d_{BET}) can be calculated for the powder using

$$d_{BET} = \frac{6}{(\rho S_v)} \quad (2)$$

where ρ is the materials density and S_v the surface area of the sample. Using the density determined from Rietveld refinement (6.648 g/cm^3), the calculated d_{BET} for the xerogel was 100 nm. The particles are not truly spherical but this is in good agreement with the average crystallite size determined from XRD peak broadening (94 nm) and the observed particle size from SEM, suggesting the majority of particles are single crystals.

Electronic Conductivity. Electrical resistivity of LSM is measured as a function of temperature and in general reported as conductivity (σ)

$$\sigma = \frac{1}{R} \quad (3)$$

where R is the bulk resistivity of the material. The temperature-dependent conductivity of LSM is reported to occur by small polaron hopping and can be expressed as

$$\sigma(T) = \frac{A}{T} e\left(\frac{-E_a}{kT}\right) \quad (4)$$

where E_a is the activation energy of the hopping mechanism, k is the Boltzmann constant, and A is the pre-exponential factor.[45] The activation energy for the conduction process is obtained from the slope of a plot of ln(σT) versus 1/T.

Conductivity measurements were made on three sintered LSM pellets prepared from calcined xerogel powder and one sintered LSM pellet prepared from commercial powder (Praxair, USA) with the reported stoichiometry $(La_{0.85}Sr_{0.15})_{0.98}MnO_3$. Two of the xerogel-derived LSM pellets, which are labeled Xero-1 and Xero-2, were prepared from LSM powder mixed with binder, and the third pellet, labeled Xero-3, was prepared without binder. The use of binder significantly improved the geometric density of the pellets, which were 94, 91, and 73% of theoretical for Xero-1, Xero-2, and Xero-3, respectively, using the density determined from Rietveld refinement. The pellet prepared from Praxair LSM, labeled Prax-1, was prepared with binder and had a geometric density of 96%. The improved geometric density for the Praxair powder is likely due to the inhomogeneous size distribution of the powder. Inhomogeneous particle sizes can improve green density of compacts because smaller submicrometer particle fill in the pore space created by the larger agglomerates, thereby leading to increased packing density. The difficulty in reaching high green densities for homogeneous nanoparticles is a known phenomenon.[18] Optimizing densification is important for measuring bulk properties but is not of concern for the predominant use of LSM, which is as a porous cathode material.[3]

Figure 8 shows ln(σT) as a function of $10^3/T$ from 1000 to 400 °C for the four LSM samples. The activation energies over the temperature range and the electronic conductivities

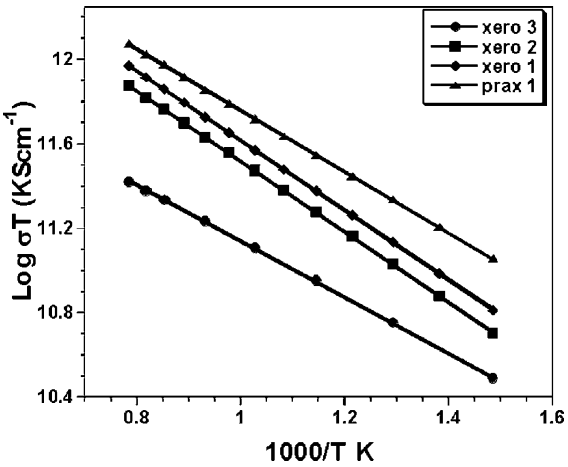

Figure 8. Plot of ln(σT) as a function of $10^4/T$ for synthesized LSM xerogel and commercial LSM powders sintered as pellets at 1400 °C for 3 h.

Table 2. Activation Energy and Conductivity Results for Sintered LSM Xerogels

sample	E_a (eV)	σ at 800 °C (Ω^{-1} cm^{-1})	σ at 1000 °C (Ω^{-1} cm^{-1})	density (g/cm^3)
Xerogel 1	0.146 ± 0.006	122 ± 6	129 ± 6	5.8961 (91%)
Xerogel 2	0.153 ± 0.005	116 ± 7	124 ± 7	6.0807 (94%)
Xerogel 3	0.126 ± 0.006	70 ± 4	72 ± 4	4.6633 (73%)
Praxair 1	0.132 ± 0.003	131 ± 6	139 ± 6	6.1281 (96%)

at 1000 and 800 °C are summarized in Table 2. The electronic conductivity at 1000 °C for Xero-1, Xero-2, and Xero-3 were 129 ± 6, 124 ± 7, and 72 ± 4 Ω^{-1} cm^{-1}, respectively. The lower conductivity for Xero-3 is expected because conductivity is known to decrease with increasing porosity.[42] Within experimental error, at 1000 °C Xero-1 and Prax-1 (139 ± 6) have the same electronic conductivity and Xero-2 has a slightly lower conductivity than Prax-1. Conductivity of the pellets at 800 °C showed a similar trend. The Praxair LSM is expected to have a slightly higher conductivity than the xerogel-derived LSM because of the higher Sr^{2+} content and the A-site deficiency in the commercial powder. Sr^{2+} substitution and A-site deficiency in LSM increase the Mn^{4+} content, and therefore the concentration of the extrinsic defect necessary for conductivity, the localized hole.[45]

The plots of ln(σT) as a function of $10^4/T$ for the four samples were linear over the entire range investigated and consistent with reports for Sr-doped lanthanum manganite. The activation energies ranged between 0.13 and 0.15 for the four samples. Within experimental error, the activation energies for Xero-1 and Xero-2 agreed and were slightly larger than those for Prax-1 and Xerogel-3. These activation energies are in agreement with literature values for $La_{1-x}Sr_xMnO_3$ with x from 0.1 to 0.15, which were between 0.1 and 0.18 eV.[42,46,47]

Conclusions

This epoxide addition method is a general technique for preparing gels of a variety of transition, rare-earth, and main group elements. We have previously demonstrated that in

(45) Vanroosmalen, J. A. M.; Huijsmans, J. P. P.; Plomp, L. *Solid State Ionics* **1993**, *66* (3−4), 279−284.

(46) Basu, R. N.; Pratihar, S. K.; Saha, M.; Maiti, H. S. *Mater. Lett.* **1997**, *32*, 217−222.

(47) Hammouche, A.; Schouler, E. J. L.; Henault, A. *Solid State Ionics* **1988**, *28−30*, 1205−1207.

mixed metal systems, such as yttria-stabilized zirconia, homogeneous gels could be formed that result in phase pure crystalline products. Here we have demonstrated that the divalent cations Mn^{2+} and Sr^{2+}, which generally do not gel with this method, can be incorporated into gel networks of La^{3+}. The morphology of the resultant xerogel was intermediated between the networked structure of the gel-forming trivalent cation and the particulate precipitates formed by the divalent cations. These results are relevant not only for the synthesis of LSM but also for the general applicability of the epoxide addition method to other mixed oxide compounds.

Acknowledgment. This work was supported by the University of California Energy Institute, the National Science Foundation (Grant DMR-0120990), and the Department of Energy (Student Employee Graduate Research Fellowship). The authors thank Alexandra Navrotsky for use of the Netzsch 449 Thermal Analyzer and the Bruker Equinox 55 TGA-IR. This work was performed under the auspices of the U.S. Department of Energy by the University of California, Lawrence Livermore National Laboratory, under Contract No. W-7405-Eng-48.

Supporting Information Available: Powder XRD profile of an LSM xerogel calcined at 1000 °C and nitrogen adsorption−desorption isotherms for an as-prepared LSM xerogel. This material is available free of charge via the Internet at http://pubs.acs.org.

CM052301J